Continuous fabrication of polymeric vesicles and nanotubes with fluidic channels

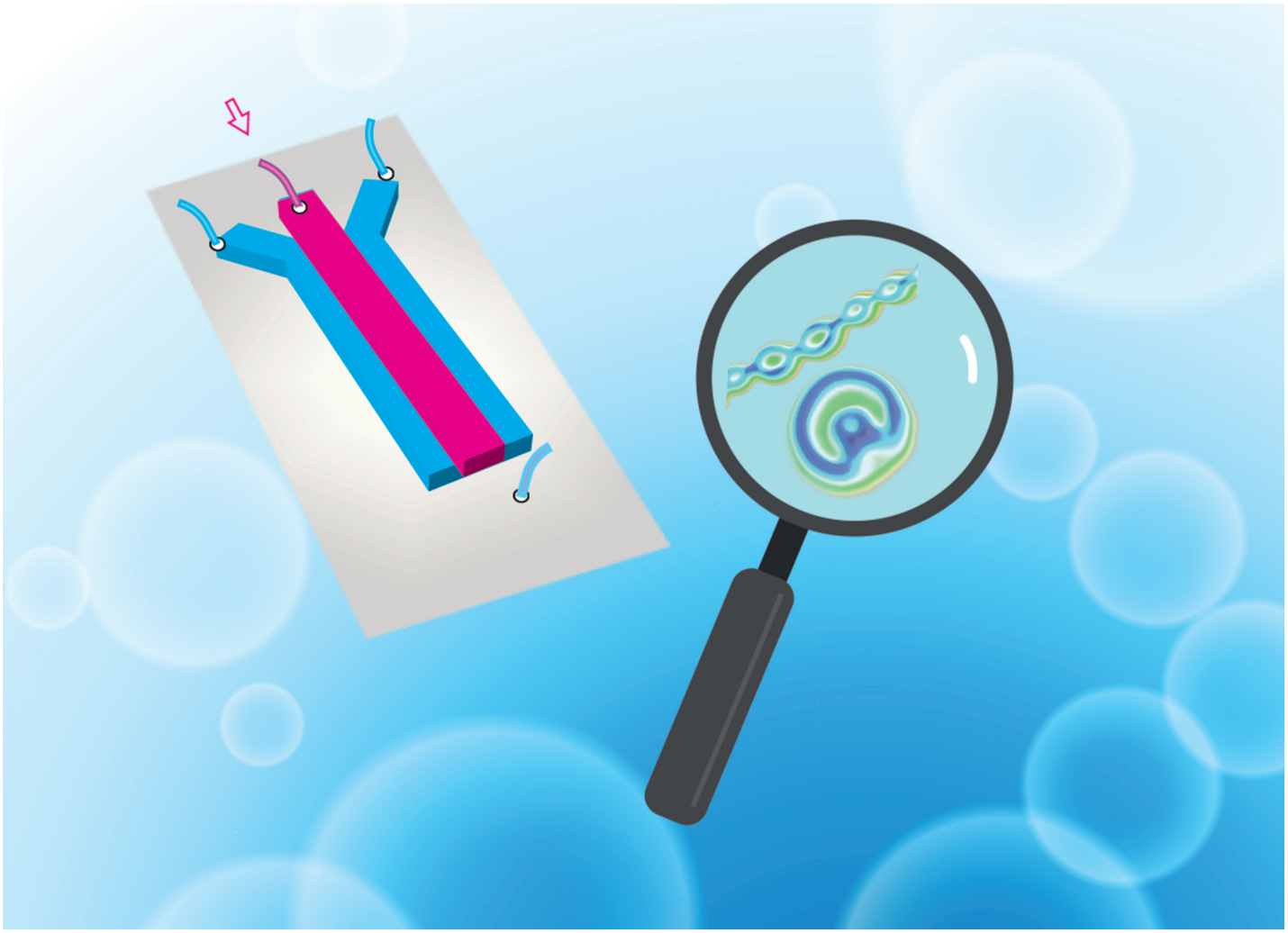

Showcasing work from the Department of Bio-organic chemistry, Institute for Molecules and Materials, Radboud University, Nijmegen, the Netherlands.

Continuous fabrication of polymeric vesicles and nanotubes with fluidic channels

Easy and continuous production of diversely shaped (sphere, bowl shaped, necklace-like) polymeric vesicles was realized with the use of a microfluidic device. By varying the flow parameters of the device, both the size and the shape of vesicles are readily tunable. The flow device also enables the fabrication of potential carriers for diverse agents ranging from small molecules to nanometer sized catalytic particles. The versatile and flexible approach can find wide applications in delivery and catalysis.

As featured in:

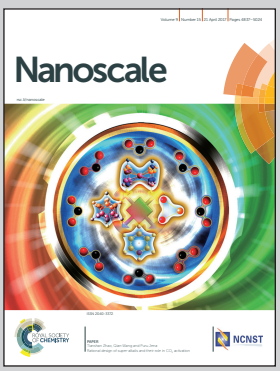

See Jan C. M. van Hest, Daniela A. Wilson *et al.*, *Nanoscale*, 2017, **9**, 4875.

ROYAL SOCIETY OF CHEMISTRY

rsc.li/nanoscale

Registered charity number: 207890

Nanoscale

COMMUNICATION

View Article Online
View Journal | View Issue

Cite this: *Nanoscale*, 2017, **9**, 4875

Received 6th January 2017,
Accepted 27th January 2017

DOI: 10.1039/c7nr00142h

rsc.li/nanoscale

Continuous fabrication of polymeric vesicles and nanotubes with fluidic channels†

Fei Peng, Nan-Nan Deng, Yingfeng Tu, Jan C. M. van Hest* and Daniela A. Wilson*

Fluidic channels were employed to induce the self-assembly of poly(ethylene glycol)-*b*-polystyrene into polymeric vesicles and nanotubes. The laminar flow in the device enables controlled diffusion of two miscible liquids at the phase boundary, leading to the formation of homogeneous polymeric structures of different shapes. These structures could be easily loaded with small molecule cargoes and functionalized with nanometer sized catalytic platinum nanoparticles. This technique offers a facile methodology to rapidly and continuously produce well-defined polymeric structures for nanotechnology applications.

Polymersomes are bilayer structures self-assembled from amphiphilic polymers.[1–3] Both lumen and polymersome membranes provide high loading efficiencies of hydrophilic and hydrophobic cargos, respectively. Being more robust and tunable[4,5] than their lipid-based counterparts, polymersomes have attracted increasing attention with regard to applications in pharmaceutics,[2] cosmetics,[6] imaging[7] and catalysis.[8] To fabricate these polymersomes, the cosolvent method[9] and the rehydration method[10,11] have been applied traditionally. These methods have the limitation that it is difficult to vary the size and they usually yield polymersomes with a broad size distribution. Post-processing steps, such as membrane extrusion[12] and sonication[13] are therefore required to reduce the polydispersity of the polymersomes produced. However, these post-treatment steps could lead to undesired material membrane interactions and loss of the encapsulated cargo.

In order to directly create polymersomes with well-defined sizes, microfluidic techniques have been developed. Weitz's group fabricated monodisperse polymersomes through droplet formation using two immiscible liquids.[14] The formed W/O/W double emulsions act as templates to form vesicles after removing the residual organic solvent.[15] Monodisperse micrometer sized vesicles were fabricated in this way.[16] To generate vesicles in the nanometer size range, laminar mixing of two miscible liquids in a fluidic channel has been shown to be a promising approach.[17–19] Well-defined nanometer sized vesicles, especially those in the range of 50 nm–200 nm, are important in drug delivery for ensuring a long circulation time *in vivo* and an optimal cellular uptake without interference of the cell metabolism.[20,21]

Besides size, shape is another important feature that can affect polymersome properties. Although a few batch processes are described to create vesicles with non-spherical morphologies,[22–27] to the best of our knowledge, no continuous flow procedures have been reported on the shape control of polymersomes. In this paper we report the use of a flow device to fabricate nanometer-sized vesicles and nanotubes through laminar mixing of a polymer organic solution and water,[28] ensuring a high production rate as well as high reproducibility. In addition, the ease of combining this vesicle production method with cargo loading makes this a versatile method for the preparation of polymeric assemblies for various applications.

For the preparation of polymeric vesicles, the amphiphilic block copolymer poly(ethylene glycol)$_{44}$-*b*-polystyrene$_{190}$ was used, which was synthesized *via* atom-transfer radical polymerization (see the Experimental section, Fig. S1 and S2†).[29,30] The flow device was used as depicted in Fig. 1. An aqueous solution was injected through two side channels while the diblock copolymer in an organic solvent (THF/dioxane) solution was introduced into the middle channel (Fig. S3†). This device is a flow-focusing channel with a continuous phase flanking the dispersed phase. Flow focusing has been used for sphere vesicle generation.[31] For the middle phase, both boundaries at the two sides are available for mixing. As both organic solvents are miscible with water, the diffusion between the two liquid phases resulted in a solution gradient, which induced self-assembly. With a traditional cosolvent method, the self-assembly process of PEG$_{44}$-*b*-PS$_{190}$ starts when the THF content drops below approximately 77%. In the fast

Institute for Molecules and Materials, Radboud University, Heyendaalseweg 135, 6525 AJ Nijmegen, The Netherlands. E-mail: d.wilson@science.ru.nl

† Electronic supplementary information (ESI) available: ^{1}H NMR/GPC spectra of the polymer, additional electron microscopy/confocal microscopy images and nanoparticle tracking analysis data as described in the text. See DOI: 10.1039/c7nr00142h

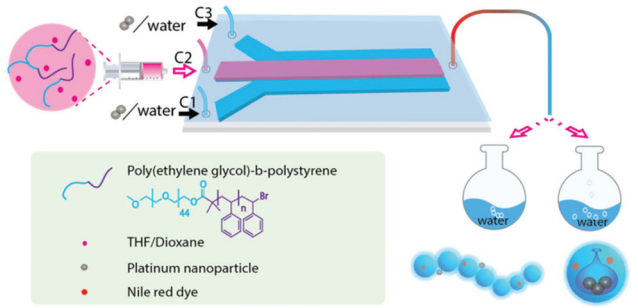

Fig. 1 The fluidic platform for the preparation of polymeric vesicles and nanotubes by varying the mode of collection and initial polymer concentration. The polymer dissolved in THF/dioxane was injected into the main channel (C2) and brought into contact with water in the two side channels (C1, C3) of the fluidic device.

fluidic system, the steep solvent gradient at the two-phase boundary led to a small distance where the THF/dioxane content dropped to this limit. This short distance as well as the high surface to volume ratio resulted in a shortened timescale of mixing.[32]

In the traditional cosolvent method, the formation of structures starts with nucleation of a few unimer polymers, followed by a diffusion limited growth in size.[33] The final step is a slow exchange of unimer polymers to reach equilibrium. To study this process, the copolymer was firstly dissolved in the organic solution in a batch experiment. Then water was delivered to it *via* a syringe pump. This process was monitored *via* a dynamic light scattering (DLS) technique in a flow mode.[34,35] Both relaxation time and vesicle formation kinetics can be derived from the plot of the scattered light intensity against time, large positive amplitudes indicating vesicle formation. In the case of the fluidic channel set-up, the calculated solvent mixing time is shorter than the aggregation time as determined from the batch experiment (for more detailed information, see Fig. S4†).

In addition, the polymer diffusion inside the organic solvent is two orders of magnitude lower than that of the two organic and aqueous phases.[36] The formation of polymeric assemblies is therefore dependent on flow rate/hydrodynamic conditions and the induced local polymer concentration, leading to kinetically trapped shapes instead of dynamic stable structures.

As the flow rate and polymer concentration are expected to play an important role in the control of self-assembly, we sought to vary the size and morphology of the structures by tuning the mixing factors employing this fluidic device. Additionally we hypothesized that maintaining the flow conditions or not during collection would also affect the final morphology, so different collection methods were studied.

As initial conditions, we used a concentration of 10 mg mL^{-1} of PEG_{44}-*b*-PS_{190} and a flow rate of C1 : C2 : C3 = 10 : 10 : 10 mL h^{-1}. The self-assembled structures were collected in two ways: (i) *via* the "insertion method" in which the collecting tube was inserted into water, and (ii) *via* the "dripping method" in which the output was dripped into water. *Via* both methods the outflow of the samples in a large excess of water led to the final vitrification of the vesicular structures. For determination of the size and shape, the collected samples were then characterized by TEM without additional processing. In the case of the "dripping method", vesicles were observed, while notably necklace-like nanotubes were generated *via* the "insertion method". There are only a few reports about tubular structures, or necklace-like nanotubes. Helmerson *et al.* described the fabrication of necklace-like nanotubes with poly (butadiene-*b*-ethylene oxide) using a combination of optical tweezer pulling and micropipetting.[25] In our case, necklace-like nanotubes could be generated in a simple and continuous way (Fig. 2A–C, for more images of nanotubes see Fig. S5A†). The nanotube membrane was clearly observed in the TEM images, reflecting its vesicular properties. The average diameter of the polymeric nanotubes was 152 nm. (The intensity profile of a vesicle unit in a polymeric nanotube is shown in Fig. 2D. The diameter of this vesicle unit was approximately 150 nm.) The average diameter at the neck of polymeric nanotubes was 45 nm. The tube length could reach 35 μm at maximum. For tuning the length of polymeric nanotubes, shearing forces (introduced by vigorous magnetic stirring) during collection were varied. When the stirring rate was increased to 500 rpm and 1000 rpm, the average tube length was decreased to 10.8 μm and 7.6 μm while the average length of tubes obtained without agitation was 14.8 μm (Fig. 3A–C). In all other cases the outflow was collected without stirring. The membrane thickness of the polymeric nanotube was close to that of spherical vesicles obtained by the dripping method (20 nm, Fig. S6†). Polymeric nanotubes were only observed with the "insertion method". Furthermore, sampling of the outflow directly from the device exit tube and fast quenching of the structures into liquid nitrogen show the presence of vesicles by TEM (Fig. S7†). This indicates that the nanotube formation occurs outside of the device. We think that the high concentration of flexible vesicles pushed by the flow and slowed down at the exit in water as well as the presence of a high concentration of the plasticizing agent in a small local volume would facilitate the colliding and merging of the vesicles. The flow direction and shear force favour the formation of one-directional polymeric nanotubes instead of merged large vesicles. The fusion could be indicated by the fact that in certain sections the neighbouring vesicle units were not completely connected but instead shared a center wall and in a hemifusion state (Fig. S8†). This was suggested previously as an intermediate state of unilamellar polymersome fusion.[37] Previous reports[38] have shown that vesicle to fused nanorod transition occurs two orders of magnitude more rapidly than its reverse way. Therefore we think that the likelihood of the first formation of giant vesicles and later fission into polymersome necklaces are relatively low.

Another possibility during the nanotube formation was previously suggested to be unimer insertion, however in a dilute batch system with no possibility for fusion.[39] In this case, the growth rate (insertion of new unimers) is faster than the birth

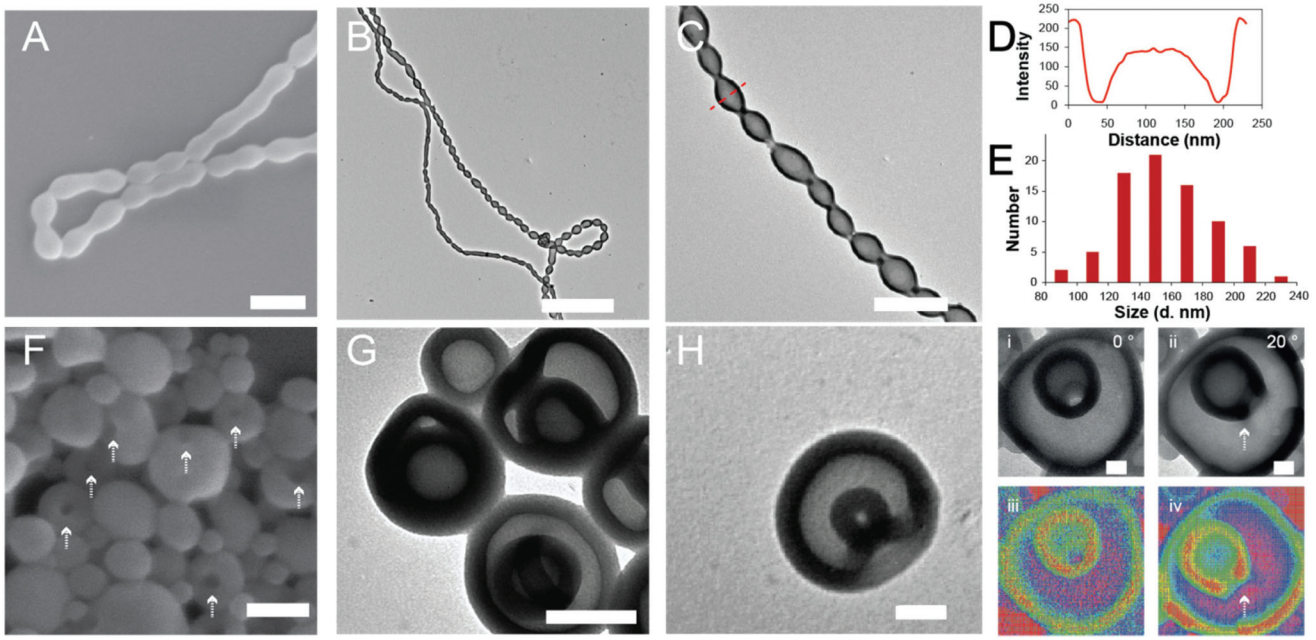

Fig. 2 (A) Scanning electron microscopy (SEM) images of polymeric nanotubes, scale bar represents 500 nm; (B) transmission electron microscopy (TEM) images of polymeric nanotubes at lower magnification (scale bar = 2 μm); (C) polymeric nanotubes at higher magnification (scale bar = 500 nm); (D) plot profile of a vesicle unit/cross section in the polymeric nanotubes indicated by the red dashed line in (C) showing the intensity as a function of distance over the cross section; (E) size/diameter distribution diagram of the vesicle units in polymeric nanotubes (80 assemblies were counted); (F) SEM images of polymeric vesicles, scale bar represents 150 nm, the white arrows pointing to the openings of stomatocyte vesicles; (G, H) TEM images of the fabricated stomatocyte vesicles, scale bar is 100 nm and 50 nm respectively; (i, ii) TEM images of a polymersome stomatocyte at a tilting angle of 0° and 20°, respectively; (note the top and side views of the stomach); (iii, iv) corresponding 3D intensity profiles of the same stomatocyte, the white arrow pointing to the opening of the stomatocyte vesicle.

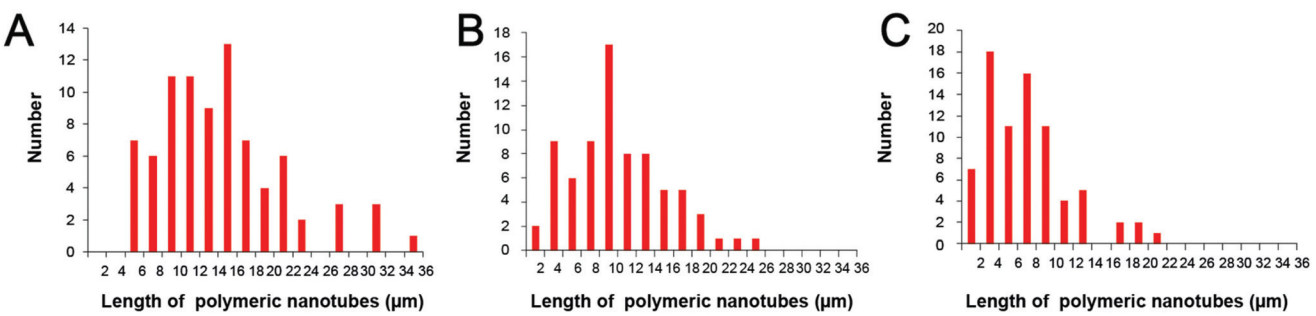

Fig. 3 TEM analysis of the length of polymeric nanotubes collected with the insertion method (A) at a stirring rate of 0 rpm; (B) at a stirring rate of 500 rpm; (C) at a stirring rate of 1000 rpm; for each analysis 80 assemblies were counted.

rate of new vesicles. Due to immiscibility of constitutional polymer chains in the bilayer vesicle membrane, one copolymer has to overcome a very high-energy barrier to move from the outer layer into the inner layer of the vesicles. Therefore the outer membrane would grow faster than the inner ones. To reduce the resulted tension, elongated structures are obtained. In this case the vesicle curvature is expected to decrease. This could be an explanation for the less curved section in the nanotubes (Fig. S8B†).

With the "dripping method", the vesicles and plasticizing agent were diluted and quenched by utilizing a large amount of water in a short time, therefore only vesicles were obtained. It is interesting to observe that among polymeric vesicles, bowl shaped vesicles/"stomatocytes" could be formed (Fig. 2F–H and S5B†). In Fig. 2F, the openings of stomatocytes are clearly shown. It is to be noted that only openings facing towards the front were visible in the SEM images. In the TEM images (Fig. 2G and H), the polymer membrane fold-in and the formed cavities were clear. The stomatocyte structure could account for a maximum of 54% in the vesicle population (based on 155 specimens assessed by TEM). The TEM of stomatocytes at different angles (top view and side view) is shown in Fig. 2i–iv, in which the top view of stomatocytes should be differentiated from the multilamellar vesicle. One possible

mechanism could be that during the fast mixing process at the interface of two liquid phases, the inner compartment of the formed spherical vesicles is still filled with THF/dioxane. With the tuned ratio of THF/dioxane, the swelling extent of PS can be so well controlled that the newly formed membrane is only permeable to an organic solvent but not to water. At the phase boundary, the solvent gradient induced organic solvent outward diffusion and evaporation of the organic solvent entrapped inside could be responsible for the formation of an osmotic gradient, leading to membrane folding and bowl-shaped structure formation.[40–42]

Besides the collecting methods, we also explored the impact of the initial polymer concentration on the morphology. We already know at a concentration of 10 mg mL^{-1} vesicles were obtained with the dripping method and nanotubes were generated with the insertion method. At a lower concentration (1 mg mL^{-1}) we found that only vesicles were observed using either the "insertion method" or the "dripping method", while nanotube structures were observed in both cases for the higher initial polymer concentration of 20 mg mL^{-1} (Fig. 4A and S9†).

Next, we explored the ability to control the size of the vesicles *via* modifying the hydrodynamic parameters. A low concentration of polymer solution (1 mg mL^{-1}) was used to avoid the formation of polymeric nanotube structures. The dripping method was used to collect the outflow from the fluidic channel. Keeping the flow ratio of the polymer solution and aqueous solution constant at 1 : 1, the vesicles experienced a decrease in diameter from 218 to 123 nm when the flow rate was elevated from 5 mL h^{-1} to 30 mL h^{-1} (Fig. 4B, DLS data). This is a result of the faster mixing process, which leads to a lower local polymer concentration available to form vesicles. The results were also confirmed with the nanoparticle tracking analysis (NTA) technique (Fig. S10†). This NTA technique allows individual particle detection with a minimum detection limit as low as 10 nm. At a constant flow rate of the polymer solution and aqueous solution at 30 mL h^{-1}, an increasing trend in size was observed when the initial polymer concentration was increased from 1 mg mL^{-1} to 10 mg mL^{-1} (Fig. 4C). In addition, with a concentration of 1 mg mL^{-1} polymer solution, the size of vesicles decreased from 214 to 189 nm when the flow ratio of the polymer solution and aqueous solution (C2 : C1/C3) was changed from 1 : 1 to 1 : 2. It should be noted that all the vesicles prepared above were narrowly distributed in size as indicated by the polydispersity value in Fig. 4C.

After obtaining the polymeric nanotube and vesicle structures, we investigated the ability to incorporate a hydrophobic cargo, by mixing the fluorescent dye Nile red with the polymer organic solution before injection into the middle channel (Fig. 5A). An initial polymer concentration of 10 mg mL^{-1} was used and the flow rate of the side and main channels was maintained at 10 mL h^{-1}. Polymeric nanotubes obtained by the insertion method and vesicles generated by the dripping

A

	polymeric structure morphology	
polymer concentration (mg/mL)	insertion method	dripping method
1	vesicles	vesicles
10	vesicles	polymeric nanotubes
20	polymeric nanotubes	polymeric nanotubes

B

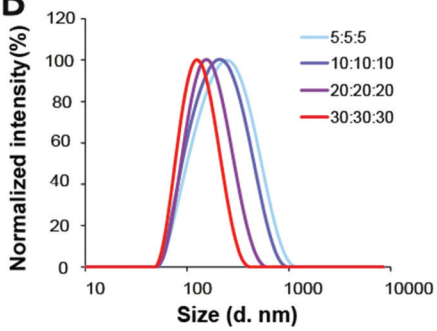

C

polymer concentration (mg/mL)	polymeric structure morphology	flow rate C1:C2:C3 (mL/h)	size (d. nm)	polydispersity index
1	vesicles	30:30:30	123.8	0.092
2	vesicles	30:30:30	130.9	0.156
3	vesicles	30:30:30	150.0	0.173
10	vesicles	30:30:30	200.9	0.169
1	vesicles	10:10:10	214.1	0.180
1	vesicles	10:5:10	189.3	0.220

Fig. 4 (A) Morphologies of polymeric structures were tuned by changing the collecting methods and polymer concentration; (B) sizes of vesicles were tuned by changing the flow rate; the particle intensity percentage was plotted against the diameter of the vesicles (dynamic light scattering (DLS) data); (C) tuning the size/diameter (DLS data) of vesicles by changing the polymer concentration and flow ratio between the main channel and side channel.

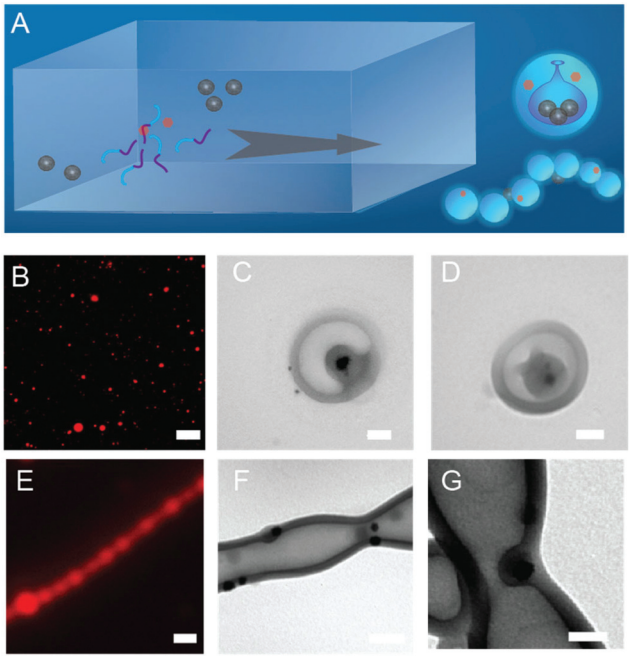

Fig. 5 (A) Schematic illustration of *in situ* loading of Nile red/platinum nanoparticles into stomatocyte vesicles and polymeric nanotubes. The Nile red/polymer in the THF/dioxane solution was injected into the main channel (C2); platinum nanoparticle aqueous solution was pumped through the two side channels (C1/C3) of the fluidic device into the main fluidic channel; (B) confocal fluorescent microscopy image of Nile red loaded vesicles, scale bar represents 2 μm; (C, D) TEM images of platinum nanoparticle loaded stomatocytes fabricated through the microfluidic method, scale bar represents 50 nm; (E) confocal fluorescent microscopy image of Nile red loaded vesicles, scale bar represents 500 nm; (F, G) TEM images of polymeric nanotubes functionalized with PVP coated platinum nanoparticles. Scale bar is 50 nm.

method could be clearly visualized with confocal fluorescence microscopy using Nile red's fluorescence (Fig. 5B and E). Since the diffraction limit of the confocal microscope is about 200 nm,[43,44] it could not be differentiated whether Nile red was localized on the membrane or the inner compartments. Besides the hydrophobic Nile red, the hydrophilic fluorescent drug doxorubicin could also be loaded (Fig. S11†).

We subsequently explored the possibility of entrapping nanoparticles in the stomatocyte and nanotube structures by addition of platinum nanoparticles (PtNPs) to the aqueous solution. The initial polymer concentration in THF/dioxane was kept at 10 mg mL^{-1}. PtNPs were fabricated through reduction of $KPtCl_4$ and capped with poly(vinylpyrrolidone) (PVP, MW: 10 000 Da).[45–47] The platinum nanoparticles were well dispersed in water (48.9 ± 3.3 nm, 5.06 ± 0.1 × 10^{11} particles per mL, Fig. S12†). With a flow rate of 10 mL h^{-1}, PtNP-loaded stomatocytes were obtained with the "dripping method" (Fig. 5C and D). The PtNP loading efficiency reached approximately 42% (TEM assessment on 50 specimens). Smaller PtNP loaded stomatocytes (189 nm) were obtained, compared to stomatocytes prepared by the conventional co-solvent method (325 nm). In previous reports inorganic nanoparticles were loaded into the membrane of polymersomes, so only nanoparticles smaller than the membrane thickness could be loaded.[48,49] In our case PtNPs were loaded in the cavity of polymersome stomatocytes. Therefore there would be no influence on the vesicle membrane and the stability of the vesicles. When the "insertion method" was applied, polymeric nanotubes were obtained which were functionalized with PtNPs (Fig. 5F and G). The PVP capped PtNPs were found to be preferentially located in the junction of the nanotube where the curvature was the highest.

Conclusions

A fast and simple method has been developed to fabricate self-assemblies with a non-spherical morphology. With our method, nanotubes and stomatocytes could be produced in a continuous and well-defined fashion. Furthermore, injection of an aqueous solution containing PtNPs into the microfluidic channel resulted in encapsulation of the particles in both types of structures. This versatile approach can be used for scaled up production of polymeric vesicles with non-spherical morphologies.

Acknowledgements

This work was supported by the European Research Council under the European Union's Seventh Framework Programme (FP7/2007-20012)/ERC-StG 307679 "StomaMotors". We acknowledge support from the Ministry of Education, Culture and Science (Gravitation program 024.001.035). N.-N. Deng acknowledges funding from the European Union's Horizon 2020 research and innovation programme under the Marie Sklodowska-Curie grant agreement No. 659907. F. Peng acknowledges funding from the China scholarship council.

References

1 B. M. Discher, Y. Y. Won, D. S. Ege, J. C. M. Lee, F. S. Bates, D. E. Discher and D. A. Hammer, *Science*, 1999, **284**, 1143–1146.
2 F. Ahmed, R. I. Pakunlu, G. Srinivas, A. Brannan, F. Bates, M. L. Klein, T. Minko and D. E. Discher, *Mol. Pharm.*, 2006, **3**, 340–350.
3 H. E. Colley, V. Hearnden, M. Avila-Olias, D. Cecchin, I. Canton, J. Madsen, S. MacNeil, N. Warren, K. Hu, J. A. McKeating, S. P. Armes, C. Murdoch, M. H. Thornhill and G. Battaglia, *Mol. Pharm.*, 2014, **11**, 1176–1188.
4 H. Bermudez, A. K. Brannan, D. A. Hammer, F. S. Bates and D. E. Discher, *Macromolecules*, 2002, **35**, 8203–8208.
5 R. Rodriguez-Garcia, M. Mell, I. Lopez-Montero, J. Netzel, T. Hellweg and F. Monroy, *Soft Matter*, 2011, **7**, 1532–1542.
6 S. H. Kim, H. C. Shum, J. W. Kim, J. C. Cho and D. A. Weitz, *J. Am. Chem. Soc.*, 2011, **133**, 15165–15171.

7 R. P. Brinkhuis, K. Stojanov, P. Laverman, J. Eilander, I. S. Zuhorn, F. P. Rutjes and J. C. van Hest, *Bioconjugate Chem.*, 2012, **23**, 958–965.
8 Z. Wang, M. C. van Oers, F. P. Rutjes and J. C. van Hest, *Angew. Chem., Int. Ed.*, 2012, **51**, 10746–10750.
9 P. L. Soo and A. Eisenberg, *J. Polym. Sci., Polym. Phys.*, 2004, **42**, 923–938.
10 J. R. Howse, R. A. Jones, G. Battaglia, R. E. Ducker, G. J. Leggett and A. J. Ryan, *Nat. Mater.*, 2009, **8**, 507–511.
11 P. P. Ghoroghchian, G. Z. Li, D. H. Levine, K. P. Davis, F. S. Bates, D. A. Hammer and M. J. Therien, *Macromolecules*, 2006, **39**, 1673–1675.
12 S. Rameez, I. Bamba and A. F. Palmer, *Langmuir*, 2010, **26**, 5279–5285.
13 P. P. Ghoroghchian, P. R. Frail, K. Susumu, D. Blessington, A. K. Brannan, F. S. Bates, B. Chance, D. A. Hammer and M. J. Therien, *P. Natl. Acad. Sci. USA*, 2005, **102**, 2922–2927.
14 H. C. Shum, J. W. Kim and D. A. Weitz, *J. Am. Chem. Soc.*, 2008, **130**, 9543–9549.
15 J. Thiele, V. Chokkalingam, S. H. Ma, D. A. Wilson and W. T. S. Huck, *Mater. Horiz.*, 2014, **1**, 96–101.
16 N. N. Deng, J. Sun, W. Wang, X. J. Ju, R. Xie and L. Y. Chu, *ACS Appl. Mater. Interfaces*, 2014, **6**, 3817–3821.
17 J. Thiele, D. Steinhauser, T. Pfohl and S. Forster, *Langmuir*, 2010, **26**, 6860–6863.
18 R. Bleul, R. Thiermann, G. U. Marten, M. J. House, T. G. St Pierre, U. O. Hafeli and M. Maskos, *Nanoscale*, 2013, **5**, 11385–11393.
19 L. Brown, S. L. McArthur, P. C. Wright, A. Lewis and G. Battaglia, *Lab Chip*, 2010, **10**, 1922–1928.
20 K. Y. Win and S. S. Feng, *Biomaterials*, 2005, **26**, 2713–2722.
21 A. Prokop and J. M. Davidson, *J. Pharm. Sci.*, 2008, **97**, 3518–3590.
22 J. Grumelard, A. Taubert and W. Meier, *Chem. Commun.*, 2004, 1462–1463.
23 J. D. Robertson, G. Yealland, M. Avila-Olias, L. Chierico, O. Bandmann, S. A. Renshaw and G. Battaglia, *ACS Nano*, 2014, **8**, 4650–4661.
24 J. He, Y. J. Liu, T. Babu, Z. J. Wei and Z. H. Nie, *J. Am. Chem. Soc.*, 2012, **134**, 11342–11345.
25 J. E. Reiner, J. M. Wells, R. B. Kishore, C. Pfefferkorn and K. Helmerson, *Proc. Natl. Acad. Sci. U. S. A.*, 2006, **103**, 1173–1177.
26 J. Raez, R. Barjovanu, J. A. Massey, M. A. Winnik and I. Manners, *Angew. Chem., Int. Ed.*, 2000, **39**, 3862–3865.
27 J. Raez, I. Manners and M. A. Winnik, *J. Am. Chem. Soc.*, 2002, **124**, 10381–10395.
28 S. Takayama, E. Ostuni, X. P. Qian, J. C. McDonald, X. Y. Jiang, P. LeDuc, M. H. Wu, D. E. Ingber and G. M. Whitesides, *Adv. Mater.*, 2001, **13**, 570–574.
29 K. T. Kim, J. J. L. M. Cornelissen, R. J. M. Nolte and J. C. M. van Hest, *Adv. Mater.*, 2009, **21**, 2787–2791.
30 F. H. Meng, G. H. M. Engbers, A. Gessner, R. H. Muller and J. Feijen, *J. Biomed. Mater. Res., Part A*, 2004, **70**, 97–106.
31 A. S. Utada, E. Lorenceau, D. R. Link, P. D. Kaplan, H. A. Stone and D. A. Weitz, *Science*, 2005, **308**, 537–541.
32 R. Karnik, F. Gu, P. Basto, C. Cannizzaro, L. Dean, W. Kyei-Manu, R. Langer and O. C. Farokhzad, *Nano Lett.*, 2008, **8**, 2906–2912.
33 B. K. Johnson and R. K. Prud'homme, *Phys. Rev. Lett.*, 2003, **91**, 118302.
34 L. Shen, J. Z. Du, S. P. Armes and S. Y. Liu, *Langmuir*, 2008, **24**, 10019–10025.
35 L. Chen, H. W. Shen and A. Eisenberg, *J. Phys. Chem. B*, 1999, **103**, 9488–9497.
36 R. Thiermann, W. Mueller, A. Montesinos-Castellanos, D. Metzke, P. Lob, V. Hessel and M. Maskos, *Polymer*, 2012, **53**, 2205–2210.
37 H. Y. Chang, Y. L. Lin, Y. J. Sheng and H. K. Tsao, *Macromolecules*, 2013, **46**, 5644–5656.
38 L. B. Luo and A. Eisenberg, *Langmuir*, 2001, **17**, 6804–6811.
39 K. Iyama and T. Nose, *Macromolecules*, 1998, **31**, 7356–7364.
40 D. A. Wilson, R. J. M. Nolte and J. C. M. van Hest, *Nat. Chem.*, 2012, **4**, 268–274.
41 F. Peng, Y. F. Tu, J. C. M. van Hest and D. A. Wilson, *Angew. Chem., Int. Ed.*, 2015, **54**, 11662–11665.
42 L. K. E. A. Abdelmohsen, M. Nijemeisland, G. M. Pawar, G. J. A. Janssen, R. J. M. Nolte, J. C. M. van Hest and D. A. Wilson, *ACS Nano*, 2016, **10**, 2652–2660.
43 Z. B. Wang, W. Guo, L. Li, B. Luk'yanchuk, A. Khan, Z. Liu, Z. C. Chen and M. H. Hong, *Nat. Commun.*, 2011, **2**, 218.
44 M. Fukuta, S. Kanamori, T. Furukawa, Y. Nawa, W. Inami, S. Lin, Y. Kawata and S. Terakawa, *Sci. Rep.*, 2015, **5**, 16068.
45 E. G. Jung, Y. Shin, M. Lee, J. Yo and T. Kang, *ACS Appl. Mater. Interfaces*, 2015, **7**, 10666–10670.
46 Y. J. Song, Y. Yang, C. J. Medforth, E. Pereira, A. K. Singh, H. F. Xu, Y. B. Jiang, C. J. Brinker, F. van Swol and J. A. Shelnutt, *J. Am. Chem. Soc.*, 2004, **126**, 635–645.
47 L. Wang and Y. Yamauchi, *J. Am. Chem. Soc.*, 2009, **131**, 9152–9153.
48 R. J. Hickey, A. S. Haynes, J. M. Kikkawa and S. J. Park, *J. Am. Chem. Soc.*, 2011, **133**, 1517–1525.
49 B. M. Geilich, A. L. van de Ven, G. L. Singleton, L. J. Sepulveda, S. Sridhar and T. J. Webster, *Nanoscale*, 2015, **7**, 3511–3519.

